ACS Macro Letters

pubs.acs.org/macroletters Viewpoint

100th Anniversary of Macromolecular Science Viewpoint: Attractive Soft Matter: Association Kinetics, Dynamics, and Pathway Complexity in Electrostatically Coassembled Micelles

Christian C. M. Sproncken, J. Rodrigo Magana, and Ilja K. Voets*

Cite This: *ACS Macro Lett.* 2021, 10, 167−179 Read Online

ACCESS | Metrics & More | Article Recommendations

ABSTRACT: Electrostatically coassembled micelles constitute a versatile class of functional soft materials with broad application potential as, for example, encapsulation agents for nanomedicine and nanoreactors for gels and inorganic particles. The nanostructures that form upon the mixing of selected oppositely charged (block co)polymers and other ionic species greatly depend on the chemical structure and physicochemical properties of the micellar building blocks, such as charge density, block length (ratio), and hydrophobicity. Nearly three decades of research since the introduction of this new class of polymer micelles shed significant light on the structure and properties of the steady-state association colloids. Dynamics and out-of-equilibrium processes, such as (dis)assembly pathways, exchange kinetics of the micellar constituents, and reaction-assembly networks, have steadily gained more attention. We foresee that the broadened scope will contribute toward the design and preparation of otherwise unattainable structures with emergent functionalities and properties. This Viewpoint focuses on current efforts to study such dynamic and out-of-equilibrium processes with greater spatiotemporal detail. We highlight different approaches and discuss how they reveal and rationalize similarities and differences in the behavior of mixed micelles prepared under various conditions and from different polymeric building blocks.

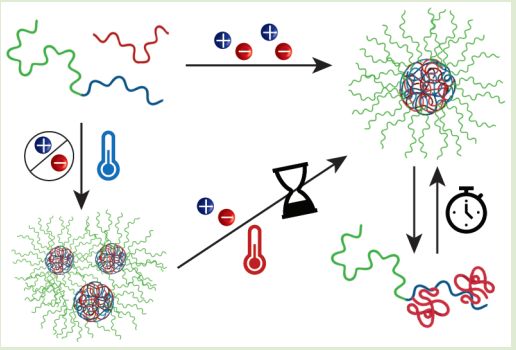

Mixing of two aqueous solutions of oppositely charged macromolecules may induce a liquid−liquid phase separation known as complex coacervation.[1] The two resulting liquids differ in the concentration of both polyelectrolytes: while the dilute phase is depleted in the macromolecules, the dense, complex coacervate phase is enriched in both. This phase separation is driven by the combination of attractive Coulombic interaction and entropic gain arising from the release of counterions.[2] The relative contribution of these driving forces is highly dependent on constituent chemistry and physical parameters such as salt concentration. Advantageously, macroscopic phase separation can be restricted to the nanometric scale to create mixed association colloids through the conjugation of an uncharged, soluble polymer block to either one or both of the charged macroions.[3] The resultant hydrocolloids are often micelles with a complex coacervate core surrounded by a neutral corona (Figure 1A). These so-called complex coacervate core micelles[4] (C3Ms) have also been coined polyion complex[3] (PIC) micelles and interpolyelectrolyte complex[5] (IPEC) micelles.

Thermodynamic aspects of complex coacervation have been covered extensively by others,[6−17] to which we refer the interested reader for a more in-depth description. Briefly, both enthalpic and entropic contributions may be significant, each of which depends markedly on the ionic strength of the solution. A polyelectrolyte chain is surrounded by a cloud of its counterions. At low ionic strength, the concentration of ions surrounding the polyion is high compared to the bulk ion concentration. The large Debye length leads to dilute counterion clouds as a compromise between Coulombic attraction and the counterion entropy. Upon addition of an oppositely charged polymer, tight complexation brings the charges closer together (Coulombic attraction; exothermic) and the counterions are released into the solution (entropy gain). On the other hand, at high ionic strength, the counterion clouds are denser, so that addition of, and complexation with, the second polymer becomes endothermic. Still, the entropy gain from counterion release results in a net energy gain for complex formation. However, above a critical salt concentration the net driving force for complexation vanishes and complex coacervation no longer takes place.

Received: November 6, 2020
Accepted: January 5, 2021
Published: January 11, 2021

https://dx.doi.org/10.1021/acsmacrolett.0c00787
ACS Macro Lett. 2021, 10, 167−179

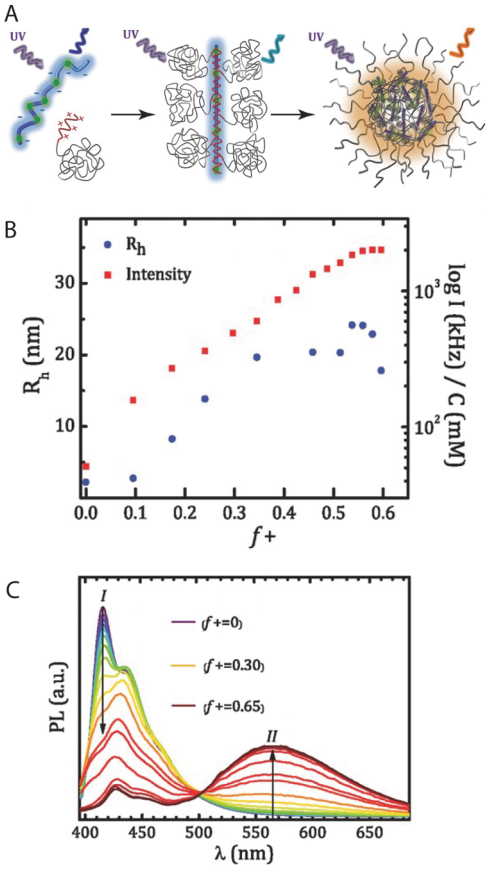

Figure 1. (A) Complex coacervate core micelles were formed from a cationic-neutral dbp and anionic hp. At $f_+ \sim 0.3$, a single hp binds multiple dbps and increasing f_+ toward 0.5 leads to the formation of condensed C3Ms. (B) Hydrodynamic radii and intensity, corrected for dilution, obtained from light scattering, both increase with increasing f_+. (C) Photoluminescence (PL) spectra with increasing f_+ (following arrows) display a shift in vibronic bands (from I to II) as a result of assembly into micelles. Adapted and reproduced with permission from Cingil et al.[59] Copyright 2016 Wiley-VCH Verlag GmbH & Co.

Besides the salt concentration, the chemical nature of the components can affect the energy balance. In addition to electrostatic interactions, hydrophobic interactions and hydrogen bond formation are often contributing driving forces.[18] Coacervation of polyelectrolytes that exhibit these additional interactions enhances the entropic and enthalpic contributions of complexation, resulting in an elevated critical salt concentration.[19,20]

The growth of micellar complex coacervates is limited to mesoscopic dimensions, provided that sufficiently long neutral solubilizing chains are attached to the polyelectrolyte chains. Neutral blocks shorter than the charged blocks to which they are conjugated usually do not suffice for micellization and instead often lead to precipitation.[4] The size of the resultant C3Ms is dictated by the same physical laws that govern the dimensions of other micelles. The free energy of the surface created by the phase separation drives the growth of the core, while the concomitant stretching of both the corona- and core-forming blocks tends to limit the micellar dimensions. The interplay between these factors determines the size-dependent free energy gain associated with micellization and thus the mean aggregation number and size of the C3Ms in equilibrium.

Over the last decades, numerous studies have shed light on the different types of coassembled micelles formed via complex coacervation of (block) copolymers and oppositely charged components.[4,21] C3Ms can be constructed by combining ionic-neutral diblock copolymers (dbp) with a plethora of oppositely charged species, including linear and branched (synthetic) polyelectrolytes, polysaccharides,[22] DNA,[23] proteins,[24] peptides,[25] dendrimers,[26] multivalent ions,[27−29] and metallic complexes.[30] Their application potential spans from materials science to nanomedicine and is largely dependent on the chemical nature of the constituent and embedded building blocks. Encapsulation of biomolecules, such as DNA, RNA, and proteins, for protective delivery and controlled release purposes is one of the most active areas of fundamental and applied research on C3Ms.[11,12,31,32] Documented benefits of this supramolecular compartmentalization include enhanced stability in the bloodstream,[33] specific targeting,[8,34] and increased cellular uptake.[35] C3Ms have also been used as confined reaction environments to produce nanoreactors and templates for the formation of, for example, nanogels[36] and inorganic nanoparticles.[37] Their intrinsic hydrophilicity, responsivity, and versatility make C3Ms an exciting class of waterborne polymer materials. Water contents up to 77% have been reported for complex coacervates,[38−40] in stark contrast to the cores of amphiphilic micelles, which contain only small amounts of water. Such high levels of hydration yield a suitable environment for the encapsulation of fragile, water-soluble, and charged compounds. The micellar carriers can be programmed to release their cargo upon changes in pH,[41] ionic strength,[42] temperature, and chemical triggers, such as sugars.[43] Dimensions, morphology, stability, and many other physicochemical and functional properties are tunable through environmental cues and composition.

The phase behavior of C3Ms has been extensively mapped, describing the influence of diblock copolymer (dbp) and homopolymer (hp) length, charge mixing ratio, and total concentration, as well as the role of ionic strength, on the final assembly.[18,44−49] In addition to steady-state properties, it is of great interest to investigate the pathways that govern C3M association and dissociation. Understanding what structures form as soon as the components are mixed and monitoring their temporal evolution to the final associated state can both provide fundamental insights on (self- and co)assembly processes in living and synthetic systems, as well as aid the design of (nano)structured functional materials. Complexes pass through various intermediate states before relaxing to the lowest energy state. The time scales of these relaxation processes vary dramatically between systems of different chemical nature and ionic strength. Kinetic traps may stall this structural evolution or prevent access to the equilibrium state altogether.

Similarly, coassembly at high (salt) concentration, followed by dilution, can produce other colloidal objects than those directly prepared at low (salt) concentration.[50] Moreover, the order of dbp/hp addition and incomplete or slow mixing alter the assembly and equilibration pathway of complex coacervates, which may significantly impact their structure and properties.[51−53] While the spatial and temporal resolution required to monitor these processes was previously unattainable, recent advances in experimental tools now allow a closer look at (dis)assembly pathways, equilibration, and reaction-assembly networks in situ. We can benefit from this opportunity and better control the formation of, for example,

https://dx.doi.org/10.1021/acsmacrolett.0c00787
ACS Macro Lett. 2021, 10, 167−179

kinetically trapped states to build a more extensive library of (nano)structured materials from the same building blocks. In this Viewpoint, we highlight recent developments and discuss exciting new research directions, focusing on dynamic and out-of-equilibrium processes, such as association and dissociation kinetics, pathway complexity, exchange dynamics, and reaction-assembly networks.

STEADY-STATE PROPERTIES

Complex coacervate core micelles form at (near-)charge stoichiometric compositions when the concentrations of positively and negatively chargeable monomers (n_+, n_-) are balanced. The composition where C3Ms are most abundant is referred to as the preferred micellar composition (PMC). For polyelectrolytes with a comparable degree of dissociation, α, the PMC typically corresponds to $f_+ = \frac{n_+}{n_+ + n_-} = 0.5$, which is equivalent to $\frac{n_+}{n_-} = 1.0$. The PMC is pH-dependent and may deviate significantly from $f_+ = 0.5$ when weak polyelectrolytes with a pH-dependent charge density are used to prepare the C3Ms. A commonly employed, alternative notation for the composition of DNA-carrying C3Ms is the phosphate-to-amine molar ratio P/N, which is not to be mistaken for the molar ratio of negative to positive charges, N/P. For clarity, we will use f_+ throughout this Viewpoint.

The morphology and size of C3Ms are dependent on the architecture of the polymeric components, their (relative) lengths,[54] mixing fraction,[55] and various other factors.[4,48] The ratio between the lengths of the corona- and core-forming blocks of the dbp, N_{corona}/N_{core},[54] and solution ionic strength[48] can be used as efficient handles to tune the morphology of the coassembled colloids. A transition from spherical ($N_{corona}/N_{core} \geq 0.9-1.0$) to wormlike micelles (WLM) to vesicular structures ($N_{corona}/N_{core} \leq 0.1-0.2$) is anticipated with decreasing N_{corona}/N_{core} under otherwise similar conditions.[4,54] Vesicles can be prepared from diblock copolymers with very short neutral blocks compared to the length of the charged blocks. Spherical C3Ms grow larger in size upon an increase in the overall molecular weight of the constituent diblock copolymers. This is mostly due to the increased length of the core-forming block, while the length of the corona-forming block plays only a minor role.[46,48] The size of C3Ms composed of a single dbp and an oppositely charged homopolymer (S-C3Ms) is also virtually independent of the length of the homopolymer[48] and dendrimer generation in dendrimicelles.[56] This insight has been exploited to custom-tailor the number of dendrimers encapsulated per C3M.[56]

The chemical nature and composition of the constituent polymers also affect micellar stability, which is compromised at high ionic strengths. This is because the cohesive interactions between oppositely charged chains weaken at elevated salt concentrations. The salt effectively acts as a plasticizer and, whereas the core may be glassy in the absence of salt, it liquefies at elevated salt concentrations.[13] Most C3Ms thus completely disassemble once a certain ionic strength is surpassed. This critical ionic strength (I_{cr}, also $c_{s,cr}$) not only depends on the types of polyions,[18,57] but also on their (relative) length.[48] Harada and Kataoka reported already in 1999 that pairs of oppositely charged block copolymers with equal cationic and anionic block lengths formed large C3Ms with a clearly separated core and corona. Mixing dbps of unmatched polyelectrolyte block lengths instead produced only the smallest possible neutral complexes.[58] Van der Burgh et al. realized that the core-forming blocks should not be too long compared to the corona-forming blocks to avoid macroscopic phase separation.[46] A $N_{corona}/N_{core} > 3$ was suggested to mitigate precipitation. Hofs et al. compared double dbp C3Ms (D-C3Ms) with S-C3Ms.[2] The S−C3Ms were found larger (R_H = 26 nm) and more resistant to salt (I_{cr} > 50 mM $NaNO_3$) than the D-C3Ms (R_H = 18 nm, I_{cr} = 50 mM $NaNO_3$). Since the cationic homopolymers were longer than the cationic blocks of the positively charged dbp, the observed differences may originate from several effects, such as increased crowding and shorter core-forming blocks in the D-C3Ms. Van der Kooij et al. showed that the critical ionic strength for S-C3Ms increases for longer (anionic) homopolymer chains until a plateau value is reached.[48] Similarly, increasing the cationic block length of cationic-neutral dbps[48] and dendrimer generation[56] leads to higher salt resistance.

Light scattering is a convenient tool to monitor the (dis)appearance of C3Ms. The static scattering intensity is proportional to the weight concentration and mean mass of the scattering objects. As f_+ is varied, a pronounced peak develops around charge stoichiometric conditions, which reveals the PMC at which the highest number of micelles is found. Based on these observations, Van der Burgh et al. proposed a speciation diagram, which describes the formation and disintegration of C3Ms into individual (co)polymers and small complexes, so-called soluble complex particles (SCPs), as a function of f_+.[46] Recently, the formation and evolution of these SCPs into micelles was studied in detail by Cingil et al. by harnessing the optical response of mechanochromic polymers with distinctly different fluorescence profiles in monomeric, complexed, and condensed states (Figure 1).[59] To this end, a conjugated anionic homopolymer was mixed with a cationic-neutral dbp at varying mixing ratios from $f_+ = 0$ up to $f_+ = 0.65$ (Figure 1A). In the absence of the copolymer at $f_+ = 0$, the molecularly dissolved mechanochromic polyanion emitted blue light (I in Figure 1C). Upon an increase in f_+ from 0 to just below 0.3, the polyanion is stretched as it binds the added cationic-neutral dbp in a bottlebrush-like manner. The formation of these complexes isdetectable by an increase in scattering intensity and hydrodynamic radius (Figure 1B) and a decrease in photoluminescence intensity (Figure 1C). A further increase beyond $f_+ = 0.3$ led to the condensation of multiples of these SCPs into larger micelles, as deduced from the emergence of new vibronic bands (II in Figure 1C). These appeardue to several mechanochromic polymer chains being in close proximity of each other within the multimolecular micellar core. We anticipate more insightful studies on the micellar state diagram, which has hitherto received little attention, using (single-molecule) fluorescence tools and other advanced characterization techniques.

ASSOCIATION AND DISSOCIATION PATHWAYS

Whereas the steady-state structure and properties of C3Ms have been widely investigated, much less is known about the (dis)assembly pathways, structural rearrangements within the (transient) complexes, chain exchange between micelles, and morphological transitions. The few studies that focus on these processes give a glimpse of the involved intricacies and reveal the untapped potential to exploit kinetic handles to create structures that are inaccessible through other means.

Most of the kinetic studies on C3Ms have focused on micellization pathways. In general, we distinguish between two

https://dx.doi.org/10.1021/acsmacrolett.0c00787
ACS Macro Lett. 2021, 10, 167−179

main mechanisms, fusion-fission and expulsion-insertion, through which initially formed transient (metastable) complexes may rearrange into steady-state (micellar) superstructures (Figure 2). Fusion-fission pertains to the emergence

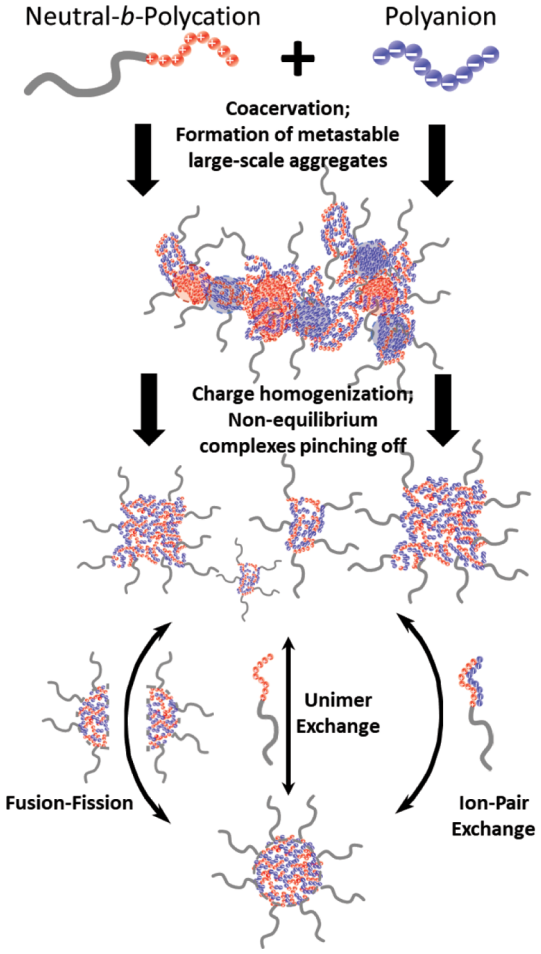

Figure 2. Schematic of the pathway for C3M formation: initially formed transient structures rearrange into smaller complexes, which equilibrate to steady-state C3Ms via (a combination of) three relaxation mechanisms. Adapted with permission from Amann et al.[63] Copyright 2019 American Chemical Society.

of thermodynamically favored structures due to the breakup and merger of "embryonic" complexes. Alternatively, steady-state aggregates may arise upon (many) expulsion and insertion events of constituent building blocks, either in unimeric form, as ion pairs, or as small soluble complexes. Which mechanism, fusion-fission or expulsion-insertion, dominates under which conditions is yet to be discovered.

Prior to the emergence of a new (condensed) phase, a transient, liquid−liquid phase separation is observed in a variety of processes, including protein crystallization,[60] mineralization,[61] and the formation of polymersomes.[62] During C3M formation, such transient structures were first reported by Cohen Stuart et al., in a pioneering light scattering study. They reveal that micellization occurs within seconds after the mixing of poly(*N*,*N*-dimethylamino ethyl methacrylate)$_{35}$-*co*-poly(glyceryl methacrylate)$_{105}$ (PDMAEMA-*co*-PGMA) and poly(acrylic acid)$_{158}$ (PAA), but is preceded by transient, macroscopic phase separation.[45]

Using state-of-the-art techniques, Lund and co-workers recently studied the early stages of S-C3M formation, combining stopped-flow mixing with a 2.6 ms dead time, with time-resolved small-angle X-ray scattering (trSAXS) experiments with an impressive time-resolution of 5 ms.[63] These trSAXS experiments also revealed transient structures; large aggregates with an inhomogeneous charge distribution formed directly after the mixing of poly(vinylbenzyl trimethylammonium chloride)$_y$-*block*-poly(ethylene oxide)$_{46}$ (PVBTA-*b*-PEO; y = 6, 8, 12, 19) and poly(sodium 4-styrenesulfonate)$_{19}$ (PSS), which rearranged over the course of seconds into smaller C3Ms (Figure 2). With increasing PVBTA block length, the observed transient complexes were larger and rearranged more slowly. Doubling the PVBTA block length from 6 to 12 monomers increased the equilibration time by more than an order of magnitude, from ∼100 ms to 30 s. When the cationic block length was further increased from 12 to 19 (matching the oppositely charged PSS block), the observed nonequilibrium state became kinetically frozen, since no relaxation occurred over time. Instead of single micelles, pearl-necklace types of clusters were found from fitting the scattering profile, and in time, the initially turbid solution phase-separated macroscopically. The authors relate this effect to multivalency. A dbp with a long ionic block has a lower dissociation probability than a dbp with a shorter one, as more noncovalent bonds must be broken for expulsion from the complex. Consequently, the ionic-neutral dbp exchange rate decreases significantly with an increasing degree of polymerization of the ionic block.

Looking further into the relaxation kinetics, the authors observed two processes with different rate constants (Figure 2). The fast process ($k_1 \sim 10\ s^{-1}$) involves chain rearrangements in the large aggregates leading to smaller clusters with a more homogeneous charge distribution. The slow process ($k_2 \sim 0.3\ s^{-1}$) is related to the reorganization into equilibrium micelles. Interestingly, this second, slow relaxation process was concentration-independent, suggesting that the equilibration is driven mainly by the exchange of polymer chains rather than fusion and fission of (pre)micelles. Tirrell and co-workers conducted time-resolved SAXS experiments on longer dbps (PVBTA$_{53}$-*b*-PEO$_{112}$ and PVBTA$_{100}$-*b*-PEO$_{225}$) mixed with the weak polyelectrolyte PAA$_{158}$.[64] In good agreement with their molecular dynamics simulations, the trSAXS experiments showed charge-neutral clusters formed within the 100 ms of experimental dead time, which rearranged into small equilibrium micelles (R_H = 10 nm) within a matter of seconds. The kinetic profiles also suggested that micellar fusion−fission events are unlikely. Conflicting, however, with the earlier findings of Cohen Stuart and Lund is the lack of larger charged aggregates in the first few ms after mixing. The Tirrell team attributes this dissimilarity to the different nature (weak vs strong) of the polyanion, but additional interactions may also play a role here. For example, $\pi-\pi$ stacking interactions may occur between the phenyl rings of the core-forming blocks in S-C3Ms composed of PVBTA-*b*-PEO/PSS, while these are absent in the S-C3Ms comprising PVBTA-*b*-PEO and PAA. The more hydrophobic character of PSS compared to PAA may further enhance the cohesive interactions within the micellar core of PSS-bearing C3Ms relative to PAA-bearing C3Ms.

Since the ionic strength influences the balance of driving forces for C3Ms formation, Zhang et al. investigated the impact of salt on the relaxation from transient to stable

https://dx.doi.org/10.1021/acsmacrolett.0c00787
ACS Macro Lett. 2021, 10, 167−179

structures by stopped-flow mixing in combination with time-resolved static light scattering (trSLS) experiments.[65] The D-C3Ms were composed of two ionic-neutral copolymers with pH-independent charge density, namely, quaternized poly-(*N*,*N*-dimethylaminoethyl methacrylate)$_{48}$ (PQDMAEMA) and PSS$_{47}$, each connected to PEO$_{113}$ in a blockwise manner. The largest C3Ms with the lowest dispersity were found around charge stoichiometry. In the first few milliseconds after mixing at $0.47 < f_+ < 0.52$, an increase in scattering intensity was observed, which plateaued within 0.4 s. This observation was interpreted as the formation of small complexes and their subsequent equilibration into stable C3Ms within the first second after mixing. The addition of salt to as much as 0.2 M NaCl slowed the relaxation, since it took up to twice as long to reach a plateau in scattering intensity. Higher salt concentrations screened the electrostatic interactions to such an extent that less and looser complexes formed (i.e., containing more water and ions). Interestingly, at low ionic strength, the rate constant of the initial relaxation from small complexes to larger micelles increased linearly with increasing dbp concentration, suggesting a significant contribution of micellar fusion-fission events. They conclude from this observation that expulsion-insertion events must be unfavorable under their conditions. These findings contrast with those of Lund and co-workers, who detected the transient formation of larger (not smaller) aggregates prior to micellization of PEO-*b*-PVBTA/PSS. This might originate from additional interactions, such as $\pi-\pi$ stacking for PVBTA and PSS, which are absent in C3Ms composed of PQDMAEMA and PSS. Moreover, Zhang et al. studied D-C3Ms (PQDMAEMA$_{48}$-*b*-PEO$_{113}$ and PSS$_{47}$-*b*-PEO$_{113}$), while Lund and co-workers investigated S-C3Ms (PVBTA$_{19}$-*b*-PEO$_{46}$ and PSS$_{19}$). Next, salt-induced dissociation kinetics were investigated by Zhang et al.[65] Upon a step increase of the salt concentration above the $c_{s,cr}$, the C3Ms disassemble. Surprisingly, they discovered from a kinetics analysis that dissociation involved two competing processes: a second-order, concentration-dependent process and a first-order, concentration-independent process. In contrast, micellization occurred via a single, second-order mechanism, deeming insertion−expulsion events unfavorable. The difference is explained by the screening of charges from the added salt in the dissociation process, lowering the energy barrier for polyion chains to fully unbind and allowing unimers to be expelled. The mechanism of dissociation, therefore, consists both of micellar fission (second-order) and chain insertion−expulsion (first-order) events.

The difference between relaxation routes for S-C3Ms versus D-C3Ms, as described above, is best understood when other factors are kept constant. In a fascinating study on striking differences in morphology and equilibration times between (otherwise similar) D-C3Ms and S-C3Ms, very slow relaxation was observed by Shah and Leon.[66] Wormlike S-C3Ms formed upon complexation of the anionic-neutral poly(acrylic acid)$_{49}$-*block*-poly(*N*-isopropylacrylamide)$_{70}$ dbp (PAA$_{49}$-*b*-PNIPAM$_{70}$) with poly(L-lysine)$_{50}$ (PLL), while the corresponding D-C3Ms, with PLL$_{50}$-*b*-PEO$_{113}$ instead of PLL$_{50}$, were spherical. Moreover, the S-C3Ms took almost 20 h to reach a steady-state, while the D-C3Ms relaxed within 6 min, which the authors attribute to the difference in micellar morphologies.

An often-employed method to ascertain whether coassembled micelles are equilibrium structures or not is to examine whether the steady-state structure and properties are identical regardless of the assembly path and processing conditions. To this end, Tirrell and co-workers investigated the dimensions of D-C3Ms prepared from PVBTA$_{100}$-*b*-PEO$_{227}$ and PSS$_{100}$-*b*-PEO$_{227}$ via two distinct pathways.[67] In their direct dissolution method, polymer solutions of the desired salt concentration are mixed, while the salt concentration is raised postmixing in the salt annealing method. Such an approach is quite unusual compared to other studies, where instead salt is added at first and removed by means of, for example, dialysis.[51,52] Interestingly, the direct dissolution resulted in a narrow distribution of C3Ms with a small size (R_H = 25 nm), which broadened over the course of months. Contrastingly, larger complexes (R_H = 100 nm) were initially observed after salt annealing, which over time equilibrated into smaller C3Ms (R_H = 25−30 nm). These observations indicate that, upon mixing the oppositely charged polymers in the absence of salt, the attractive interactions are so strong that kinetically trapped complexes form in which part of the PEO blocks are possibly buried. The subsequent addition of salt enables the rearrangement of these complexes into thermodynamically favored smaller micelles, with a coacervate core and PEO corona. Their observations are a good example of how the conditions of preparation dictate the formation of transient structures. Kinetically trapped structures may on the one hand present an obstacle, but could on the other hand provide otherwise inaccessible nanostructures. Looking at the coassembly process with high spatiotemporal detail is therefore of great importance.

Tirrell and co-workers investigated the processes involved in salt-induced C3M dissociation using complementary trSLS experiments and theoretical modeling.[68] Upon elevation of the salt concentration, from no added salt to 0.5 M NaCl, the micellar radius was increased, within the measurement dead time of 1 s. Next, a steep drop in intensity, along with a decrease of the radius, is observed, and finally, the intensity plateaus. Their theoretical model, derived from complex coacervate scaling laws, disentangles the dissociation process into three stages. The model first predicts that the observed increase in micellar radius is the result of an uptake of more water and ions. In a second step, the micellar cores start to break apart, while fission is favored over unimer expulsion in this process. This outcome concurs with the steep decrease in intensity, as would be expected for micelles breaking in two rather than slowly losing small amounts of polymer via expulsion. The final stage described in the model is the complete separation of the coronas of these newly formed complexes, which occurs with a negligible relaxation time, accompanied by an entropy increase.

MORPHOLOGICAL TRANSITIONS

Time-resolved experiments are not only useful to study the formation and dissociation of C3Ms, but also to understand how one micellar morphology transforms into another upon variations in, for example, composition, temperature, and salt concentration. For micelles assembled from amphiphiles, such transitions are typically induced by changes in temperature and upon cosolvent addition, which affect the solvency and hence the effective packing parameter of the amphiphiles. C3M morphology is further tunable through variations in mixing fraction and salt concentration, which impact the electrostatic interactions between the constituent building blocks and, hence, the micellization free energy.

https://dx.doi.org/10.1021/acsmacrolett.0c00787
ACS Macro Lett. 2021, 10, 167−179

Takahashi et al. have shown how a dbp excess can induce a vesicle-to-micelle transition for D-C3Ms comprising the ionic blocks poly(sodium 2-acrylamido-2-methylpropanesulfonate)$_{293}$ (PAMPS) and poly(3-methacryloylaminopropyl trimethylammonium chloride)$_{215}$ (PMAPTAC) in the micellar core and the short zwitterionic block poly(2-methacryloyloxy ethyl phosphorylcholine)$_{22}$ (PMPC) in the corona.[69] Because $N_{corona}/N_{core} \sim 0.1$, vesicles form ($d$ = 200 nm in 0.1 M NaCl) near charge stoichiometry. When one of the dbps is added in excess (f_+ = 0.4 or 0.8), the vesicles transform into smaller spherical micelles (d = 44 nm). This transition is reversible upon addition of the minority dbp to restore charge stoichiometry. In a follow-up study, the authors prepared wormlike D-C3Ms from PAMPS$_{198}$-*b*-PMPC$_{22}$ and PMAPTAC$_{206}$-*b*-PMPC$_{22}$ at f_+ = 0.55 (d = 35 nm in 0.01 M NaCl).[69] TrSAXS reveals that these cylinders break down into smaller micelles with the same diameter over a time of 150 s upon addition of excess PAMPS$_{198}$-*b*-PMPC$_{22}$ to reach f_+ = 0.35. Two scenarios have been proposed for such worm-to-sphere transitions. The end of the cylindrical micelles could pinch off to release spherical micelles, or the WLM may breakup stochastically at any location. The first scenario has been observed previously for cylindrical micelles of amphiphilic polymers.[70] Takahashi et al., however, find that these WLMs dissociate into spherical C3Ms through random scission along the length of the cylinders, since a steep drop in intensity is observed, consistent with breakup of the cylinders into smaller, spherical micelles. The structural transition is reversible upon addition of PMAPTAC$_{206}$-*b*-PMPC$_{22}$ to restore f_+ = 0.55. Moreover, the sphere-to-cylinder transition is slower than the cylinder-to-sphere transition. First, within the 2.5 ms experimental dead time, short cylindrical micelles form in coexistence with the already present spheres. Then, the growth of these nascent cylinders is a slow process, with almost no observed change for the first 10 min and taking up to a full day to reach a steady state. This marked difference for the reverse transition is attributed to a high activation energy associated with slow cylinder growth.

Because of the influence of salt on the interaction strength of C3Ms, tuning the ionic strength presents another handle to transition between morphologies. Van der Kooij et al. reported on the morphological transitions observed at elevated salt concentrations (c_{NaCl} > 0.1 M) for mixed micelles containing PAA and poly(*N*-methyl-2-vinylpyridinium iodide)$_{41}$-*block*-poly(ethylene oxide)$_{204}$ (PM2VP$_{41}$-*b*-PEO$_{204}$).[48] For relatively short homopolymer chains (N_{PAA} < 50), a transition from spherical micelles to more elongated structures is observed, before the micelles finally disintegrate above the critical ionic strength. Such a morphological transition is absent in C3Ms carrying long homopolymer chains (N_{PAA} < 130) and was attributed by the authors to the entropic penalty originating from stretching of the polyanion chain.

Transitions between morphologies can also be induced upon changes in temperature due to the thermoresponsive building blocks of C3Ms. An established example is the use of poly(*N*-isoproylacrylamide) (PNIPAM or PNIPAAm) as a neutral block, which has a lower critical solution temperature (LCST ~ 32 °C). As such, increasing the temperature of aqueous solutions of D-C3Ms of PAA$_{49}$-*b*-PNIPAM$_{70}$ and PLL$_{50}$-*b*-PEO$_{113}$ above this LCST induced a (partially) reversible transition into core−shell−corona structures.[66] Contrastingly, the PAA$_{49}$-*b*-PNIPAM$_{70}$/PLL$_{50}$ system undergoes aggregation of the (wormlike) S-C3Ms. Then, upon cooling, these rearranged into spherical C3Ms with larger dimensions than those observed prior to heating. Contrary to an earlier study by Voets et al. on D-C3Ms of PAA$_{55}$-*b*-PNIPAM$_{88}$ and PM2VP$_{38}$-*b*-PEO$_{211}$,[71] Shah and Leon deduced that the coacervate remained in the core that, at T > LCST, is covered by collapsed PNIPAM chains.[66] The core−shell−corona structures reported by Voets et al. contained instead a PNIPAM core with a coacervate shell.

EXCHANGE DYNAMICS

Exchange of material between (pre)micelles is of great importance to achieve equilibration of the nanostructures and their properties. Systems might be kinetically trapped and unable to equilibrate when the exchange rates of the building blocks are very low, thus, we may not observe a transition on the experimental time scale. Species that can be exchanged include unimers, ion pairs, and small neutral complexes. Both the rate of exchange as well as the nature of the exchanging species impact the level of protection offered by the C3Ms upon encapsulating sensitive components. For example, (therapeutic) proteins and polynucleotides encapsulated within S-C3Ms (i.e., being C3Ms comprising dbp complexed with proteins, DNA, or RNA with or without auxiliary hp) are transiently exposed during material exchange between these S-C3Ms if the predominant exchange mechanism is expulsion−insertion of either small neutral complexes or individual constituents. In vivo, this transient solvent-exposure would render the water-soluble, biomacromolecular cargo packaged within C3Ms more vulnerable to degradation by proteases or nucleases than hydrophobic cargo encapsulated within amphiphilic systems. On the other hand, if fusion−fission processes dominate exchange, shielding may remain sufficient to offer the required protection of the cargo. Understanding how relative rates of expulsion−insertion and fusion−fission events depend on the properties of the building blocks greatly aids the design of, for example, encapsulation agents for nanomedicine. Since the exchange is dependent on the relative interaction strength, factors such as (changes in) salt concentration will influence the type and rate of exchange. Displacement of charged macromolecules from complexes by competitive species (i.e., polyelectrolyte chains of similar nature, but different length, compared to those in the complex) was studied by simulations and shown to be faster for larger competitive species, as well as at higher salt concentration.[72] Such factors must be considered in the choice of polymeric components.

To monitor the dynamic properties of protein−polymer C3Ms, Nolles et al. prepared spherical C3Ms with a radius of 35 nm at pH 9 from fluorescent proteins (FPs) with a net negative charge of approximately −10 and PM2VP$_{128}$-*b*-PEO$_{477}$.[73] Both the formation of C3Ms and the exchange of material between micelles occurred via association and dissociation of small, near-neutral protein−polymer complexes (i.e., SCPs) consisting of 1 dbp and around 10 FPs. To track the exchange of FPs between the micelles through Förster resonance energy transfer (FRET), the authors mixed solutions of C3Ms with either donor or acceptor FPs. When the two types of proteins were mixed and confined in the micellar core, a high FRET signal is observed, while it is reduced in the case of smaller complexes. The coexistence of these small complexes and the C3Ms presents a vulnerability of the protein cargo, when intended for delivery in vivo. Moreover, increasing the salt concentration from 0 to 20 mM, the

https://dx.doi.org/10.1021/acsmacrolett.0c00787
ACS Macro Lett. 2021, 10, 167−179

reduction in FRET signal indicated that almost half of the C3Ms had dissociated, possibly into small complexes. Such poor salt stability makes them unsuitable for use under physiological conditions, corresponding to an ionic strength around 140 mM. The stability can be improved to overcome this impediment to biomedical applications, through the incorporation of auxiliary homopolymers,[74,75] protein supercharging,[76] tethering of charged polypeptides,[77] complementary nonelectrostatic interactions,[78] and cross-linking of the polymeric shell.[79,80] The impact of these strategies on exchange dynamics and loading efficiency is yet to be investigated in-depth.

The ability of polyelectrolyte chains to adapt their conformation in equilibrated S-C3Ms was investigated by Murmiliuk et al. using fluorescence quenching experiments.[81] C3Ms were prepared from poly(methacrylic acid)$_{1267}$ (PMA) homopolymers tagged with an umbelliferone fluorescent label at their chain ends and poly[3,5-bis(trimethylammonium methyl)-4-hydroxystyrene iodide]$_{167}$-*block*-poly(ethylene oxide)$_{320}$ copolymers (QNPHOS$_{167}$-*b*-PEO$_{320}$). The system was designed as such because the QNPHOS will quench the fluorescence of the umbelliferone, which can occur either statically or dynamically. In the case of static quenching, a nonfluorescent complex forms between the dye and the cationic monomer. Dynamic quenching occurs upon collisions between the QNPHOS and the umbelliferone in its excited state, hence, requiring freedom of movement of the participating species. In the presence of excess PMA, most fluorescently labeled chains were free in solution or forming small complexes, leading to low quenching efficiency. Contrastingly, the equilibrium spherical C3Ms that were obtained at stoichiometric mixing ratio exhibit both increased static and dynamic quenching. This is expected for static quenching since the species are brought in close proximity to one another. More surprising is the 10-fold increase in dynamic quenching efficiency. The authors conclude that this result indicates that the polyelectrolyte chains retain their mobility inside the core, allowing for collisions between QNPHOS and the fluorophore.

Macrorheology revealed the major impact of salt concentration, as well as of hydrogen bond formation, on the relaxation dynamics of viscoelastic, macroscopically phase-separated complex coacervates.[82,83] Rescaling of the rheological data allowed accessing otherwise unavailable time scales via salt-time superposition. It would be of great interest to extend these studies to C3Ms and directly compare the exchange dynamics of micellar coacervates with the relaxation dynamics of macroscopic coacervates. Through a quantitative comparison of experimental results on micellar coacervates with theoretical descriptions established for macroscopic coacervates, Van der Kooij et al. deduced that the stability of macro- and mesoscopic coacervates is similar and much more dependent on the chain length of the ionic blocks than on the absence/presence of the solubilizing neutral blocks.[48]

Li et al. compared the polyion exchange rates for small, off-stoichiometric, soluble complexes (f_+ = 0.17) comprising two homopolymers to those of S-C3Ms with identical ionic blocks and formed under the same conditions.[84] Their poly(*N*-ethyl-4-vinylpyridinium bromide)$_{55}$ (PEVP$_{55}$) formed SCPs with a 16 nm radius when combined with PMA$_{1560}$, while C3Ms with radii of 25 nm were obtained when mixing with PMA$_{180}$-*b*-PEO$_{170}$. Fluorescence quenching as a result of the coupling of the cationic monomers to fluorescein dyes attached to PMA monomers (dye/monomer ∼ 1:750) was monitored to extract polyion exchange rates. Surprisingly, the higher exchange rates were found for the C3Ms compared to the SCPs. The latter contain excess PMA chains and thus, free hp chains in solution have to overcome the repulsive barrier to be exchanged with a chain in the complex. Nonstoichiometric conditions were employed in this study to form SCPs instead of macroscopic complex coacervates. Further studies are needed to elucidate the similarities and differences in the exchange processes of stoichiometric SCPs and C3Ms.

Insights from experimental studies help us understand the relation between the C3M building blocks and their exchange dynamics. Theory and simulations can complement and further advance these insights on the one hand and guide synthesis efforts and experimental design on the other hand through predictions. Bos and Sprakel employed Langevin dynamics simulations to study chain exchange between S-C3Ms composed of cationic-neutral block copolymers and anionic homopolymers, each with 20 charged monomers. The main mechanisms, expulsion−insertion and fusion−fission events, were investigated. Whereas for amphiphilic micelles, unimers are commonly exchanged between micelles, the expulsion of a single polyelectrolyte unimer is unfavored. Instead, for C3Ms, small (near-)neutral complexes are expelled and inserted. Therefore, the authors find that when the polyion lengths are exactly matched and thus the smallest neutral complex consists of only two chains, many expulsion and insertion events occur. The number of fission and fusion events is found to be orders of magnitude lower. Importantly, increasing the nonelectrostatic interaction between the two polymers significantly decreases expulsion−insertion and fission, while fusion events seem less affected by it. In contrast with simulations, experiments often involve polymers with some dispersity and slight inequalities in (block) lengths. In their simulations, by varying the ratio between the anionic and the cationic chain lengths, Bos and Sprakel demonstrated that the rates of expulsion and insertion steeply dropped. This effect is attributed to the smallest neutral complex now consisting of multiple chains, rather than only two. More ionic bonds have to be broken for the small complex to leave the micelle, decreasing the probability of expulsion. The number of fission events does not follow this trend but rather increases for shorter anionic hps, while increasing for longer hps. From this result, the authors conclude that the rearrangement of ionic bonds is more facile for short hp chains. Overall, expulsion−insertion events were found to dominate the exchange rate, over fission−fusion events. In the extreme case where the homopolymer is very long compared to the charged block of the dbp, micelles with only a few hp chains in the core could form. Such a situation could lead to a dominance of fusion−fission events because the smallest near-neutral complexes that can be expelled are on the order of the size of the C3M.

We anticipate that future work on exchange and displacement dynamics will also exploit contrast variation in small-angle neutron scattering (SANS). This powerful tool has revealed a wealth of information on the exchange dynamics of micelles from polymeric amphiphiles.[85−89] To this end, solutions of hydrogenated and (partially) deuterated micelles are mixed after which the disappearance of their characteristic scattering profiles due to exchange processes is monitored over time.[90] Harnessing this technique allows the derivation of both the mechanisms and the rates that govern exchange in C3M equilibration.

https://dx.doi.org/10.1021/acsmacrolett.0c00787
ACS Macro Lett. 2021, 10, 167−179

MULTIRESPONSIVE C3MS

A principle advantage of mixed micelles is the ease with which multiple functionalities can be combined within one and the same association colloid simply through mixing of multiple types of building blocks. This strategy has been employed to create multiresponsive micelles, which adapt to external cues such as pH,[91,92] salt concentration,[82] and temperature.[93−95] Low salt concentrations can be used to plasticize and high salt concentrations to vitrify the obtained structures, as desired. This allows for the on-demand reconfiguration and preservation of structures created using additional cues, such as heat, even when these are no longer maintained. The use of various types of (partially) immiscible components creates multicompartment micelles comprising mixed cores and demixed shells[96] or, vice versa, demixed cores and mixed shells.[5] As a result of demixing of the components, one can obtain Janus micelles,[97] core−shell−corona micelles (i.e., onion-like micelles),[71,98−100] and patchy micelles.[101]

Plamper and co-workers investigated the complexation kinetics of a system that is thermoresponsive, resulting in different structures based on the temperature of the assembly.[94] The D-C3Ms were prepared from two copolymers, $[PQDMAEMA_{17}]_4$-*star*-PEO_{114} and poly(vinylsulfonate)$_{31}$-*block*-poly(*N*-isopropylacrylamide)$_{27}$ (PVS-*b*-PNIPAM), where both the ionic blocks and the neutral stabilizing blocks were of a different type. TrSAXS performed below the LCST of PNIPAM (20 °C in 0.3 M NaCl) during mixing of the polymers revealed the formation of C3Ms within 0.13 s, with a radius of gyration of 8 nm, similar to those of samples left to equilibrate for days. Above the LCST, the PVS-*b*-PNIPAM copolymer is amphiphilic and assembles into micelles with a PNIPAM core and a highly charged PVS corona. Therefore, after mixing, these micelles complex with the oppositely charge polymer-forming multicompartmental micelles. The core−shell−corona micelles that form in this manner initially possess a rather stretched PEO corona, which relaxes within half a minute, via internal rearrangements, along with an increase in water content of both the complex coacervate and the PNIPAM core.

Kinetically trapped intermediate states in assembly pathways markedly slow down or even prohibit access to the minimum energy configuration. These metastable states often complicate the robust preparation of equilibrium superstructures with a well-defined structure and properties. It may also be a blessing in disguise, as it offers, in addition to thermodynamic handles, kinetic knobs to tune the structure and properties of mixed micelles. Owing to the electrostatic interactions governing polyelectrolyte complexation, salt type and concentration greatly influence bond strength and dynamics and, consequently, can be used to access dynamic equilibrium structures or, instead, to create interesting, semipermanent metastable architectures. The Plamper group exploited this strategy to obtain kinetically stable, nonequilibrium structures.[102] Careful tuning of the assembly temperature to values above and below the LCST, followed by a decrease in salt concentration, allowed them to kinetically trap various (coexisting) morphologies, including spherical and wormlike micelles, as well as vesicles, all from the same building blocks. Subsequent salt addition triggered the rearrangement and relaxation of these kinetically frozen nanostructures toward their equilibrium counterparts.

REACTION ASSEMBLY NETWORKS

Controlling the transient assembly behavior of amphiphilic block copolymers during polymerization has undoubtedly become a new paradigm in material science to produce nanostructured materials in kinetically arrested states. This approach, so-called polymerization-induced self-assembly (PISA), consists of the in situ chain extension of a living solvophilic polymer via reversible addition−fragmentation chain-transfer (RAFT) with a (soluble) monomer that forms a solvophobic block.[103−106] The growth of the second block drives the assembly of the copolymer into nanoparticles. Continuous changes in the molecular architecture (i.e., packing parameters) during the chain extension result in kinetic traps that are not attainable by simply dissolving these polymers.

Recently, the PISA approach was extended to double hydrophilic block copolymers by chain extending a charged block from a water-soluble macromolecular chain transfer agent (macroCTA) in the presence of an oppositely charged polyelectrolyte. This new variant was coined as polymerization-induced electrostatic self-assembly (PIESA).[107] Here, complex coacervation between the homopolymer with the growing dbp takes place during polymerization. Interestingly, the interaction between the living polymer and the oppositely charged polyelectrolytes immobilizes the growing-chain CTAs and, consequently, slows down the chain-growth rate. In PIESA, each reaction coordinate in these reaction-assembly networks thus corresponds to a different distribution of the polymerizable ionic monomers over the growing dbp chains and the solution. Consequentially, both the composition of the diblock copolymer (N_{corona}/N_{core}) and of the system (f_+) evolve over time (Note that f_+ relates exclusively to the chargeable monomers incorporated within the polymers). This often results in a gradual change in micellar morphology during PIESA, provided that the reaction conditions allow for reconfigurations to take place. These transitions originate from (at least) three different effects that occur simultaneously during PIESA. As the monomer conversion increases, (1) the mixing fraction f_+ changes, (2) the overall ionic strength is reduced as the charged monomers (which could act akin to microions) are depleted upon incorporation within the growing chains, and (3) the N_{corona}/N_{core} block length ratio of the dbp changes. Moreover, the cohesive interactions within the C3Ms grow stronger with increasing length of the polyelectrolyte block, which results in more stable structures and decelerates exchange dynamics.[48]

An illustrative example of the variety of assembled structures usually generated during PIESA due to the temporal variations in composition is shown in Figure 3.[107] In this PIESA study, Cai and co-workers employed aqueous RAFT using poly(2-hydroxypropyl methacrylamide)$_{175}$ (PHPMA) macro-CTA with a cationic monomer (2-aminoethylacrylamide hydrochloride, AEAM) by irradiation with visible light at 25 °C to yield a growing chain of PHPMA-*b*-AEAM in the presence of poly(sodium 2-acrylamido-2-methylpropanesulfonate)$_{91}$ (PAMPS).[107] It is important to notice that this reaction takes place at much higher concentrations (i.e., 25 wt %) than those generally used to form C3Ms via direct mixing and that there is a 2-fold excess of AEAM compared to the AMPS monomer concentration. Here, spherical C3Ms form at monomer conversions well below 50% conversion (non-stoichiometric conditions). When reaching charge neutralization near 50% monomer conversion, the reaction mixture

https://dx.doi.org/10.1021/acsmacrolett.0c00787
ACS Macro Lett. 2021, 10, 167−179

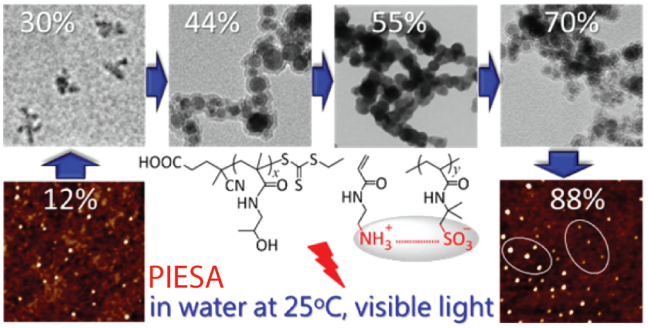

Figure 3. Morphological evolution of polyelectrolyte complexes obtained at different monomer conversions (indicated in percentages) during polymerization induced electrostatic self-assembly of $PHPMA_{175}$-*b*-$PAEAM_y$ and $PAMPS_{91}$. Note that $y = 87$ corresponds to 44% conversion. Reprinted with permission from Yu et al.[107] Copyright 2015 American Chemical Society.

forms a gel network comprised of spherical-like aggregates of about 100 nm in radius. The observed gelation may be related to the relatively high C3M volume fraction. At even higher monomer conversions, the complexes become increasingly charged, so that the network breaks up and the system reverts to a viscous liquid due to the increased electrostatic repulsion and solubilization of the chains. Interestingly, gelation was absent upon direct mixing of the two polymers postsynthesis. Instead, spherical micelles of about 40 nm in radius form upon addition of the anionic hp to the dbp after ∼50% monomer conversion.

PIESA has also been applied to chain extend dbps in the presence of ionic micelles,[108] polynucleotides,[109] and for the preparation of neutral-anionic-cationic terpolymers.[110] Vesicles or unstable lamellae were observed in many cases. It is likely related to the targeted $N_{corona}/N_{core} < 1$ of many of these reports, which typically yields vesicles or nonstable systems.[46] Moreover, the excess of block copolymer present after surpassing stoichiometry can also destabilize the assembly via bridging. The combination of these effects cannot be fully deconvoluted from the influence of the growing living polymer chain on the morphology of the complex coacervates obtained. We foresee that further experimental designs that ensure full charge stoichiometry during the whole reaction landscape and form stable complex coacervates with lower N_{core}/N_{corona} are a promising strategy for further understanding and development of PIESA.

CONCLUSION AND PERSPECTIVE

The electrostatic coassembly of (diblock) copolymers with oppositely charged species received widespread attention in the last decades as a versatile approach to create a new class of polymer micelles with interesting properties. Understanding and tuning steady-state structure−function relations through chemical and physical factors under precisely controlled conditions has been the main focus. This has greatly advanced our insight in the behavior of C3Ms and served as a solid foundation for several new fascinating research directions which are rapidly gaining ground. We anticipate a growing interest in macroscopic materials prepared from C3Ms and coacervates, such as hydrogels, thin films, adhesives, and saloplastics. Their steady-state properties are well-studied including their dependence on choice of one or two block copolymers, polymer length (ratios) and chemical nature of the components. It is yet to be elucidated how exactly such factors influence the dynamic properties of C3Ms. Conflicting results claim different mechanisms dominate the relaxation from transient structures to (steady-state) micelles. When exactly fusion-fission or expulsion-insertion mechanism govern the kinetics of C3M formation will become clear by more systematic studies. Since salt concentration affects the balance of driving forces for complexation, both the micellar stability and their dynamics are altered by it. Additional interactions in the core, such as hydrogen bonding or hydrophobic effects, contribute to the pathways and time scale of relaxation from transient to stable structures. Specifically for the use of C3Ms as carrier of biomacromolecules, simply looking at steady-state properties and stability does not paint the full picture. C3Ms composed of polypeptides (e.g., proteins) or polynucleotides, combined with ionic-neutral copolymers, must protect their sensitive cargo from deterioration in vivo. Exchange kinetics studies will shed more light on the mechanism by which these building blocks are exchanged between micelles and on the time they spend exposed. This knowledge will aid the design of C3Ms with enhanced delivery efficiency.

The formation of kinetically trapped states has long been seen as a bottleneck, but is now also embraced as an effective means to create various nanostructures with unprecedented complexity from identical building blocks. Another important development is the shift in focus from equilibrium to out-of-equilibrium conditions. The (dis)assembly kinetics and exchange dynamics of these mixed micelles are being studied in-depth using time-resolved scattering tools and fluorescence spectroscopy. These studies disclose transient (nano)-structures, which may be annealed or vitrified in the future to broaden the scope of attainable architectures. Particularly appealing in this respect are reaction-assembly networks, which disclose the role of kinetic factors and compositional variations in the assembly pathways. In addition, they hold great promise as an efficient platform for the preparation of colloidally stable nanostructures of various shapes and dimensions in high yield, because of the high concentrations that can be used.

Advances in characterization and the adoption of single-molecule tools such as single-molecule localization microscopy will shed light on the relevance of minority species in ensembles and the fate of C3Ms under out-of-equilibrium conditions, at nonstoichiometric compositions,[111,112] and in a cellular context.[113] Use of such techniques will also advance the design of C3Ms for targeted delivery of therapeutics.

Finally, we foresee an increasing effort from the polymer chemistry community to prepare and incorporate custom-tailored materials and substitute PEO by other stabilizers, such as zwitterionic/antifouling blocks,[114] to fine-tune the stability, responsivity, dynamicity, and functionality of C3Ms in vitro and in vivo for improved performance in complex (biological) environments.

AUTHOR INFORMATION

Corresponding Author

Ilja K. Voets − *Laboratory of Self-Organizing Soft Matter, Department of Chemical Engineering and Chemistry and Institute for Complex Molecular Systems, Eindhoven University of Technology, 5600 MB Eindhoven, The Netherlands;* orcid.org/0000-0003-3543-4821; Email: i.voets@tue.nl

https://dx.doi.org/10.1021/acsmacrolett.0c00787
ACS Macro Lett. 2021, 10, 167−179

Authors

Christian C. M. Sproncken − *Laboratory of Self-Organizing Soft Matter, Department of Chemical Engineering and Chemistry and Institute for Complex Molecular Systems, Eindhoven University of Technology, 5600 MB Eindhoven, The Netherlands;* orcid.org/0000-0001-5303-0519

J. Rodrigo Magana − *Laboratory of Self-Organizing Soft Matter, Department of Chemical Engineering and Chemistry and Institute for Complex Molecular Systems, Eindhoven University of Technology, 5600 MB Eindhoven, The Netherlands;* orcid.org/0000-0001-8637-1467

Complete contact information is available at: https://pubs.acs.org/10.1021/acsmacrolett.0c00787

Author Contributions

The manuscript was written through contributions of all authors.

Funding

The authors are grateful to The Netherlands Organization for Scientific Research (NWO TA Grant No. 731.015.205 and NWO LIFT Grant 731.017.407) for financial support.

Notes

The authors declare no competing financial interest.

■ ACKNOWLEDGMENTS

The authors acknowledge Chendan Li and Dr. Bas van Ravensteijn for fruitful discussions, especially on the topic of reaction assembly networks.

■ REFERENCES

(1) Bungenberg de Jong, H. G.; Kruyt, H. R. Coacervation (Partial Miscibility in Colloid Systems). *Proc. Natl. Acad. Sci. Amsterdam* **1929**, *32*, 849−856.

(2) Hofs, B.; Voets, I. K.; De Keizer, A.; Cohen Stuart, M. A. Comparison of Complex Coacervate Core Micelles from Two Diblock Copolymers or a Single Diblock Copolymer with a Polyelectrolyte. *Phys. Chem. Chem. Phys.* **2006**, *8* (36), 4242−4251.

(3) Harada, A.; Kataoka, K. Formation of Polyion Complex Micelles in an Aqueous Milieu from a Pair of Oppositely-Charged Block Copolymers with Poly(Ethylene Glycol) Segments. *Macromolecules* **1995**, *28* (15), 5294−5299.

(4) Voets, I. K.; de Keizer, A.; Cohen Stuart, M. A. Complex Coacervate Core Micelles. *Adv. Colloid Interface Sci.* **2009**, *147−148*, 300−318.

(5) Pergushov, D. V.; Müller, A. H. E.; Schacher, F. H. Micellar Interpolyelectrolyte Complexes. *Chem. Soc. Rev.* **2012**, *41* (21), 6888−6901.

(6) Shakya, A.; Girard, M.; King, J. T.; De La Cruz, M. O. Role of Chain Flexibility in Asymmetric Polyelectrolyte Complexation in Salt Solutions. *Macromolecules* **2020**, *53* (4), 1258−1269.

(7) Blocher McTigue, W. C.; Perry, S. L. Protein Encapsulation Using Complex Coacervates: What Nature Has to Teach Us. *Small* **2020**, *16* (27), 1907671.

(8) Cabral, H.; Miyata, K.; Osada, K.; Kataoka, K. Block Copolymer Micelles in Nanomedicine Applications. *Chem. Rev.* **2018**, *118*, 6844−6892.

(9) Harada, A.; Kataoka, K. Polyion Complex Micelle Formation from Double-Hydrophilic Block Copolymers Composed of Charged and Non-Charged Segments in Aqueous Media. *Polym. J.* **2018**, *50*, 95−100.

(10) Sing, C. E.; Perry, S. L. Recent Progress in the Science of Complex Coacervation. *Soft Matter* **2020**, *16* (12), 2885−2914.

(11) Horn, J. M.; Kapelner, R. A.; Obermeyer, A. C. Macro- and Microphase Separated Protein-Polyelectrolyte Complexes: Design Parameters and Current Progress. *Polymers (Basel, Switz.)* **2019**, *11* (4), 578.

(12) Chen, F.; Stenzel, M. H. Polyion Complex Micelles for Protein Delivery. *Aust. J. Chem.* **2018**, *71* (10), 768.

(13) Zhang, Y.; Batys, P.; O'Neal, J. T.; Li, F.; Sammalkorpi, M.; Lutkenhaus, J. L. Molecular Origin of the Glass Transition in Polyelectrolyte Assemblies. *ACS Cent. Sci.* **2018**, *4* (5), 638−644.

(14) Gineste, S.; Di Cola, E.; Amouroux, B.; Till, U.; Marty, J.-D.; Mingotaud, A.-F.; Mingotaud, C.; Violleau, F.; Berti, D.; Parigi, G.; Luchinat, C.; Balor, S.; Sztucki, M.; Lonetti, B. Mechanistic Insights into Polyion Complex Associations. *Macromolecules* **2018**, *51* (4), 1427−1440.

(15) Rathee, V. S.; Sidky, H.; Sikora, B. J.; Whitmer, J. K. Role of Associative Charging in the Entropy-Energy Balance of Polyelectrolyte Complexes. *J. Am. Chem. Soc.* **2018**, *140* (45), 15319−15328.

(16) Rumyantsev, A. M.; Zhulina, E. B.; Borisov, O. V. Scaling Theory of Complex Coacervate Core Micelles. *ACS Macro Lett.* **2018**, *7* (7), 811−816.

(17) Takemoto, H.; Miyata, K.; Hattori, S.; Ishii, T.; Suma, T.; Uchida, S.; Nishiyama, N.; Kataoka, K. Acidic PH-Responsive SiRNA Conjugate for Reversible Carrier Stability and Accelerated Endosomal Escape with Reduced IFNα-Associated Immune Response. *Angew. Chem., Int. Ed.* **2013**, *52* (24), 6218−6221.

(18) van der Gucht, J.; Spruijt, E.; Lemmers, M.; Cohen Stuart, M. A. Polyelectrolyte Complexes: Bulk Phases and Colloidal Systems. *J. Colloid Interface Sci.* **2011**, *361* (2), 407−422.

(19) Stapert, H. R.; Nishiyama, N.; Jiang, D. L.; Aida, T.; Kataoka, K. Polyion Complex Micelles Encapsulating Light-Harvesting Ionic Dendrimer Zinc Porphyrins. *Langmuir* **2000**, *16* (21), 8182−8188.

(20) Sadman, K.; Wang, Q.; Chen, Y.; Keshavarz, B.; Jiang, Z.; Shull, K. R. Influence of Hydrophobicity on Polyelectrolyte Complexation. *Macromolecules* **2017**, *50* (23), 9417−9426.

(21) Magana, J. R.; Sproncken, C. C. M.; Voets, I. K. On Complex Coacervate Core Micelles: Structure-Function Perspectives. *Polymers (Basel, Switz.)* **2020**, *12* (9), 1953.

(22) De Kruif, C. G.; Weinbreck, F.; De Vries, R. Complex Coacervation of Proteins and Anionic Polysaccharides. *Curr. Opin. Colloid Interface Sci.* **2004**, *9*, 340−349.

(23) Lueckheide, M.; Vieregg, J. R.; Bologna, A. J.; Leon, L.; Tirrell, M. V. Structure-Property Relationships of Oligonucleotide Polyelectrolyte Complex Micelles. *Nano Lett.* **2018**, *18* (11), 7111−7117.

(24) Mills, C. E.; Obermeyer, A.; Dong, X.; Walker, J.; Olsen, B. D. Complex Coacervate Core Micelles for the Dispersion and Stabilization of Organophosphate Hydrolase in Organic Solvents. *Langmuir* **2016**, *32* (50), 13367−13376.

(25) Wen, H.; Zhou, J.; Pan, W.; Li, Z.; Liang, D. Assembly and Reassembly of Polyelectrolyte Complex Formed by Poly(Ethylene Glycol)-Block-Poly(Glutamate Sodium) and S5R4 Peptide. *Macromolecules* **2016**, *49* (12), 4627−4633.

(26) Yang, J.; Zhang, Q.; Chang, H.; Cheng, Y. Surface-Engineered Dendrimers in Gene Delivery. *Chem. Rev.* **2015**, *115*, 5274−5300.

(27) Wu, K.; Shi, L.; Zhang, W.; An, Y.; Zhu, X.-X.; Zhang, X.; Li, Z. Formation of Hybrid Micelles between Poly(Ethylene Glycol)-Block-Poly(4-Vinylpyridinium) Cations and Sulfate Anions in an Aqueous Milieu. *Soft Matter* **2005**, *1* (6), 455.

(28) Sanson, N.; Bouyer, F.; Destarac, M.; In, M.; Gérardin, C. Hybrid Polyion Complex Micelles Formed from Double Hydrophilic Block Copolymers and Multivalent Metal Ions: Size Control and Nanostructure. *Langmuir* **2012**, *28* (8), 3773−3782.

(29) Carl, N.; Prévost, S.; Schweins, R.; Houston, J. E.; Morfin, I.; Huber, K. Invertible Micelles Based on Ion-Specific Interactions of Sr2+ and Ba2+ with Double Anionic Block Copolyelectrolytes. *Macromolecules* **2019**, *52* (22), 8759−8770.

(30) Facciotti, C.; Saggiomo, V.; van Hurne, S.; Bunschoten, A.; Kaup, R.; Velders, A. H. Oxidant-Responsive Ferrocene-Based Cyclodextrin Complex Coacervate Core Micelles. *Supramol. Chem.* **2020**, *32* (1), 30−38.

(31) Yoon, H.; Dell, E. J.; Freyer, J. L.; Campos, L. M.; Jang, W. D. Polymeric Supramolecular Assemblies Based on Multivalent Ionic Interactions for Biomedical Applications. *Polymer* **2014**, *55*, 453−464.
(32) Gao; Holkar; Srivastava. Protein−Polyelectrolyte Complexes and Micellar Assemblies. *Polymers (Basel, Switz.)* **2019**, *11* (7), 1097.
(33) Smith, A. E.; Sizovs, A.; Grandinetti, G.; Xue, L.; Reineke, T. M. Diblock Glycopolymers Promote Colloidal Stability of Polyplexes and Effective PDNA and SiRNA Delivery under Physiological Salt and Serum Conditions. *Biomacromolecules* **2011**, *12* (8), 3015−3022.
(34) Qian, Y.; Zha, Y.; Feng, B.; Pang, Z.; Zhang, B.; Sun, X.; Ren, J.; Zhang, C.; Shao, X.; Zhang, Q.; Jiang, X. PEGylated Poly(2-(Dimethylamino) Ethyl Methacrylate)/DNA Polyplex Micelles Decorated with Phage-Displayed TGN Peptide for Brain-Targeted Gene Delivery. *Biomaterials* **2013**, *34* (8), 2117−2129.
(35) Tan, Z.; Jiang, Y.; Zhang, W.; Karls, L.; Lodge, T. P.; Reineke, T. M. Polycation Architecture and Assembly Direct Successful Gene Delivery: Micelleplexes Outperform Polyplexes via Optimal DNA Packaging. *J. Am. Chem. Soc.* **2019**, *141* (40), 15804−15817.
(36) De Santis, S.; Diociaiuti, M.; Cametti, C.; Masci, G. Hyaluronic Acid and Alginate Covalent Nanogels by Template Cross-Linking in Polyion Complex Micelle Nanoreactors. *Carbohydr. Polym.* **2014**, *101* (1), 96−103.
(37) Seo, E.; Lee, S. H.; Lee, S.; Choi, S. H.; Hawker, C. J.; Kim, B. S. Highly Stable Au Nanoparticles with Double Hydrophilic Block Copolymer Templates: Correlation Between Structure and Stability. *Polym. Chem.* **2017**, *8* (31), 4528−4537.
(38) Krogstad, D. V.; Choi, S. H.; Lynd, N. A.; Audus, D. J.; Perry, S. L.; Gopez, J. D.; Hawker, C. J.; Kramer, E. J.; Tirrell, M. V. Small Angle Neutron Scattering Study of Complex Coacervate Micelles and Hydrogels Formed from Ionic Diblock and Triblock Copolymers. *J. Phys. Chem. B* **2014**, *118* (45), 13011−13018.
(39) Ortony, J. H.; Choi, S. H.; Spruell, J. M.; Hunt, J. N.; Lynd, N. A.; Krogstad, D. V.; Urban, V. S.; Hawker, C. J.; Kramer, E. J.; Han, S. Fluidity and Water in Nanoscale Domains Define Coacervate Hydrogels. *Chem. Sci.* **2014**, *5* (1), 58−67.
(40) Fu, J.; Fares, H. M.; Schlenoff, J. B. Ion-Pairing Strength in Polyelectrolyte Complexes. *Macromolecules* **2017**, *50* (3), 1066−1074.
(41) Cingil, H. E.; Meertens, N. C. H.; Voets, I. K. Temporally Programmed Disassembly and Reassembly of C3Ms. *Small* **2018**, *14* (46), 1802089.
(42) Lindhoud, S.; De Vries, R.; Schweins, R.; Cohen Stuart, M. A.; Norde, W. Salt-Induced Release of Lipase from Polyelectrolyte Complex Micelles. *Soft Matter* **2009**, *5* (1), 242−250.
(43) Ren, J.; Zhang, Y.; Zhang, J.; Gao, H.; Liu, G.; Ma, R.; An, Y.; Kong, D.; Shi, L. PH/Sugar Dual Responsive Core-Cross-Linked PIC Micelles for Enhanced Intracellular Protein Delivery. *Biomacromolecules* **2013**, *14* (10), 3434−3443.
(44) Kabanov, A. V.; Bronich, T. K.; Kabanov, V. A.; Yu, K.; Eisenberg, A. Soluble Stoichiometric Complexes from Poly(N -Ethyl-4-Vinylpyridinium) Cations and Poly(Ethylene Oxide)- Block -Polymethacrylate Anions. *Macromolecules* **1996**, *29*, 6797−6802.
(45) Cohen Stuart, M. A.; Besseling, N. A. M.; Fokkink, R. G. Formation of Micelles with Complex Coacervate Cores. *Langmuir* **1998**, *14*, 6846−6849.
(46) van der Burgh, S.; de Keizer, A.; Cohen Stuart, M. A. Complex Coacervation Core Micelles. Colloidal Stability and Aggregation Mechanism. *Langmuir* **2004**, *20* (4), 1073−1084.
(47) Voets, I. K.; De Vries, R.; Fokkink, R.; Sprakel, J.; May, R. P.; De Keizer, A.; Cohen Stuart, M. A. Towards a Structural Characterization of Charge-Driven Polymer Micelles. *Eur. Phys. J. E: Soft Matter Biol. Phys.* **2009**, *30*, 351−359.
(48) Van Der Kooij, H. M.; Spruijt, E.; Voets, I. K.; Fokkink, R.; Cohen Stuart, M. A.; Van Der Gucht, J. On the Stability and Morphology of Complex Coacervate Core Micelles: From Spherical to Wormlike Micelles. *Langmuir* **2012**, *28* (40), 14180−14191.
(49) Aloi, A.; Guibert, C.; Olijve, L. L. C.; Voets, I. K. Morphological Evolution of Complex Coacervate Core Micelles Revealed by IPAINT Microscopy. *Polymer* **2016**, *107*, 450−455.
(50) Fresnais, J.; Lavelle, C.; Berret, J. F. Nanoparticle Aggregation Controlled by Desalting Kinetics. *J. Phys. Chem. C* **2009**, *113* (37), 16371−16379.
(51) Qi, L.; Fresnais, J.; Berret, J. F.; Castaing, J. C.; Destremaut, F.; Salmon, J. B.; Cousin, F.; Chapel, J. P. Influence of the Formulation Process in Electrostatic Assembly of Nanoparticles and Macromolecules in Aqueous Solution: The Interaction Pathway. *J. Phys. Chem. C* **2010**, *114* (39), 16373−16381.
(52) Qi, L.; Fresnais, J.; Berret, J. F.; Castaing, J. C.; Grillo, I.; Chapel, J. P. Influence of the Formulation Process in Electrostatic Assembly of Nanoparticles and Macromolecules in Aqueous Solution: The Mixing Pathway. *J. Phys. Chem. C* **2010**, *114* (30), 12870−12877.
(53) Blocher McTigue, W. C.; Voke, E.; Chang, L.-W.; Perry, S. L. The Benefit of Poor Mixing: Kinetics of Coacervation. *Phys. Chem. Chem. Phys.* **2020**, *22* (36), 20643.
(54) Sakamoto, S.; Sanada, Y.; Sakashita, M.; Nishina, K.; Nakai, K.; Yusa, S. I.; Sakurai, K. Chain-Length Dependence of Polyion Complex Architecture Bearing Phosphobetaine Block Explored Using SAXS and FFF-MALS. *Polym. J.* **2014**, *46* (9), 617−622.
(55) Yan, Y.; Besseling, N. A. M.; De Keizer, A.; Drechsler, M.; Fokkink, R.; Cohen Stuart, M. A. Wormlike Aggregates from a Supramolecular Coordination Polymer and a Diblock Copolymer. *J. Phys. Chem. B* **2007**, *111* (40), 11662−11669.
(56) Wang, J.; Voets, I. K.; Fokkink, R.; van der Gucht, J.; Velders, A. H. Controlling the Number of Dendrimers in Dendrimicelle Nanoconjugates from 1 to More than 100. *Soft Matter* **2014**, *10* (37), 7337−7345.
(57) Voets, I. K.; De Keizer, A.; Cohen Stuart, M. A.; Justynska, J.; Schlaad, H. Irreversible Structural Transitions in Mixed Micelles of Oppositely Charged Diblock Copolymers in Aqueous Solution. *Macromolecules* **2007**, *40* (6), 2158−2164.
(58) Harada, A.; Kataoka, K. Chain Length Recognition: Core-Shell Supramolecular Assembly from Oppositely Charged Block Copolymers. *Science (Washington, DC, U. S.)* **1999**, *283* (5398), 65−67.
(59) Cingil, H. E.; Boz, E. B.; Wang, J.; Cohen Stuart, M. A.; Sprakel, J. Probing Nanoscale Coassembly with Dual Mechanochromic Sensors. *Adv. Funct. Mater.* **2016**, *26* (9), 1420−1427.
(60) Dumetz, A. C.; Chockla, A. M.; Kaler, E. W.; Lenhoff, A. M. Protein Phase Behavior in Aqueous Solutions: Crystallization, Liquid-Liquid Phase Separation, Gels, and Aggregates. *Biophys. J.* **2008**, *94* (2), 570−583.
(61) Wallace, A. F.; Hedges, L. O.; Fernandez-Martinez, A.; Raiteri, P.; Gale, J. D.; Waychunas, G. A.; Whitelam, S.; Banfield, J. F.; De Yoreo, J. J. Microscopic Evidence for Liquid-Liquid Separation in Supersaturated CaCO3 Solutions. *Science (Washington, DC, U. S.)* **2013**, *341* (6148), 885−889.
(62) Ianiro, A.; Wu, H.; van Rijt, M. M. J.; Vena, M. P.; Keizer, A. D. A.; Esteves, A. C. C.; Tuinier, R.; Friedrich, H.; Sommerdijk, N. A. J. M.; Patterson, J. P. Liquid−Liquid Phase Separation during Amphiphilic Self-Assembly. *Nat. Chem.* **2019**, *11* (4), 320−328.
(63) Amann, M.; Diget, J. S.; Lyngsø, J.; Pedersen, J. S.; Narayanan, T.; Lund, R. Kinetic Pathways for Polyelectrolyte Coacervate Micelle Formation Revealed by Time-Resolved Synchrotron SAXS. *Macromolecules* **2019**, *52* (21), 8227−8237.
(64) Wu, H.; Ting, J. M.; Yu, B.; Jackson, N. E.; Meng, S.; De Pablo, J. J.; Tirrell, M. V. Spatiotemporal Formation and Growth Kinetics of Polyelectrolyte Complex Micelles with Millisecond Resolution. *ACS Macro Lett.* **2020**, *9*, 1674−1680.
(65) Zhang, J.; Chen, S.; Zhu, Z.; Liu, S. Stopped-Flow Kinetic Studies of the Formation and Disintegration of Polyion Complex Micelles in Aqueous Solution. *Phys. Chem. Chem. Phys.* **2014**, *16* (1), 117−127.
(66) Shah, S.; Leon, L. Structural Transitions and Encapsulation Selectivity of Thermoresponsive Polyelectrolyte Complex Micelles. *J. Mater. Chem. B* **2019**, *7* (41), 6438−6448.
(67) Wu, H.; Ting, J. M.; Werba, O.; Meng, S.; Tirrell, M. V. Non-Equilibrium Phenomena and Kinetic Pathways in Self-Assembled Polyelectrolyte Complexes. *J. Chem. Phys.* **2018**, *149* (16), 163330.

https://dx.doi.org/10.1021/acsmacrolett.0c00787
ACS Macro Lett. 2021, 10, 167−179

(68) Wu, H.; Ting, J. M.; Tirrell, M. V. Mechanism of Dissociation Kinetics in Polyelectrolyte Complex Micelles. *Macromolecules* **2020**, *53* (1), 102−111.
(69) Takahashi, R.; Narayanan, T.; Yusa, S. I.; Sato, T. Kinetics of Morphological Transition between Cylindrical and Spherical Micelles in a Mixture of Anionic-Neutral and Cationic-Neutral Block Copolymers Studied by Time-Resolved SAXS and USAXS. *Macromolecules* **2018**, *51* (10), 3654−3662.
(70) Burke, S. E.; Eisenberg, A. Kinetics and Mechanisms of the Sphere-to-Rod and Rod-to-Sphere Transitions in the Ternary System PS310-b-PAA52/Dioxane/Water. *Langmuir* **2001**, *17* (21), 6705−6714.
(71) Voets, I. K.; Moll, P. M.; Aqil, A.; Jérôme, C.; Detrembleur, C.; De Waard, P.; De Keizer, A.; Cohen Stuart, M. A. Temperature Responsive Complex Coacervate Core Micelles with a PEO and PNIPAAm Corona. *J. Phys. Chem. B* **2008**, *112* (35), 10833−10840.
(72) Peng, B.; Muthukumar, M. Modeling Competitive Substitution in a Polyelectrolyte Complex. *J. Chem. Phys.* **2015**, *143* (24), 243133.
(73) Nolles, A.; Hooiveld, E.; Westphal, A. H.; Van Berkel, W. J. H.; Kleijn, J. M.; Borst, J. W. FRET Reveals the Formation and Exchange Dynamics of Protein-Containing Complex Coacervate Core Micelles. *Langmuir* **2018**, *34* (40), 12083−12092.
(74) Lindhoud, S.; de Vries, R.; Norde, W.; Cohen Stuart, M. A. Structure and Stability of Complex Coacervate Core Micelles with Lysozyme. *Biomacromolecules* **2007**, *8* (7), 2219−2227.
(75) Kembaren, R.; Fokkink, R.; Westphal, A. H.; Kamperman, M.; Kleijn, J. M.; Borst, J. W. Balancing Enzyme Encapsulation Efficiency and Stability in Complex Coacervate Core Micelles. *Langmuir* **2020**, *36* (29), 8494−8502.
(76) Obermeyer, A. C.; Mills, C. E.; Dong, X. H.; Flores, R. J.; Olsen, B. D. Complex Coacervation of Supercharged Proteins with Polyelectrolytes. *Soft Matter* **2016**, *12* (15), 3570−3581.
(77) Kapelner, R. A.; Obermeyer, A. C. Ionic Polypeptide Tags for Protein Phase Separation. *Chem. Sci.* **2019**, *10* (9), 2700−2707.
(78) Tabandeh, S.; Leon, L. Engineering Peptide-Based Polyelectrolyte Complexes with Increased Hydrophobicity. *Molecules* **2019**, *24* (5), 868.
(79) Yang, Y.; Zhu, H.; Wang, J.; Fang, Q.; Peng, Z. Enzymatically Disulfide-Crosslinked Chitosan/Hyaluronic Acid Layer-by-Layer Self-Assembled Microcapsules for Redox-Responsive Controlled Release of Protein. *ACS Appl. Mater. Interfaces* **2018**, *10* (39), 33493−33506.
(80) Wang, Y.; Cheng, Y. T.; Cao, C.; Oliver, J. D.; Stenzel, M. H.; Chapman, R. Polyion Complex-Templated Synthesis of Cross-Linked Single-Enzyme Nanoparticles. *Macromolecules* **2020**, *53* (13), 5487−5496.
(81) Murmiliuk, A.; Matějíček, P.; Filippov, S. K.; Janata, M.; Šlouf, M.; Pispas, S.; Štěpánek, M. Formation of Core/Corona Nanoparticles with Interpolyelectrolyte Complex Cores in Aqueous Solution: Insight into Chain Dynamics in the Complex from Fluorescence Quenching. *Soft Matter* **2018**, *14* (37), 7578−7585.
(82) Spruijt, E.; Sprakel, J.; Lemmers, M.; Cohen Stuart, M. A.; Van Der Gucht, J. Relaxation Dynamics at Different Time Scales in Electrostatic Complexes: Time-Salt Superposition. *Phys. Rev. Lett.* **2010**, *105* (20), 1−4.
(83) Marciel, A. B.; Srivastava, S.; Tirrell, M. V. Structure and Rheology of Polyelectrolyte Complex Coacervates. *Soft Matter* **2018**, *14* (13), 2454−2464.
(84) Li, Y.; Bronich, T. K.; Chelushkin, P. S.; Kabanov, A. V. Dynamic Properties of Block Ionomer Complexes with Polyion Complex Cores. *Macromolecules* **2008**, *41* (15), 5863−5868.
(85) Choi, S. H.; Lodge, T. P.; Bates, F. S. Mechanism of Molecular Exchange in Diblock Copolymer Micelles: Hypersensitivity to Core Chain Length. *Phys. Rev. Lett.* **2010**, *104* (4), 047802.
(86) Pedersen, J. S.; Hamley, I. W.; Ryu, C. Y.; Lodge, T. P. Contrast Variation Small-Angle Neutron Scattering Study of the Structure of Block Copolymer Micelles in a Slightly Selective Solvent at Semidilute Concentrations. *Macromolecules* **2000**, *33* (2), 542−550.
(87) Lund, R.; Willner, L.; Stellbrink, J.; Lindner, P.; Richter, D. Logarithmic Chain-Exchange Kinetics of Diblock Copolymer Micelles. *Phys. Rev. Lett.* **2006**, *96* (6), 068302.
(88) Lund, R.; Willner, L.; Richter, D.; Dormidontova, E. E. Equilibrium Chain Exchange Kinetics of Diblock Copolymer Micelles: Tuning and Logarithmic Relaxation. *Macromolecules* **2006**, *39* (13), 4566−4575.
(89) Lund, R.; Willner, L.; Richter, D.; Lindner, P.; Narayanan, T. Kinetic Pathway of the Cylinder-to-Sphere Transition in Block Copolymer Micelles Observed in Situ by Time-Resolved Neutron and Synchrotron Scattering. *ACS Macro Lett.* **2013**, *2* (12), 1082−1087.
(90) Carl, N.; Prévost, S.; Schweins, R.; Huber, K. Contrast Variation of Micelles Composed of Ca2+ and Block Copolymers of Two Negatively Charged Polyelectrolytes. *Colloid Polym. Sci.* **2020**, *298* (7), 663−679.
(91) Ramasamy, T.; Kim, J. H.; Choi, J. Y.; Tran, T. H.; Choi, H. G.; Yong, C. S.; Kim, J. O. PH Sensitive Polyelectrolyte Complex Micelles for Highly Effective Combination Chemotherapy. *J. Mater. Chem. B* **2014**, *2* (37), 6324−6333.
(92) Poggi, E.; Guerlain, C.; Debuigne, A.; Detrembleur, C.; Gigmes, D.; Hoeppener, S.; Schubert, U. S.; Fustin, C.-A.; Gohy, J.-F. Stimuli-Responsive Behavior of Micelles Prepared from a Poly(Vinyl Alcohol)-Block-Poly(Acrylic Acid)-Block-Poly(4-Vinylpyridine) Triblock Terpolymer. *Eur. Polym. J.* **2015**, *62*, 418−425.
(93) Dähling, C.; Lotze, G.; Drechsler, M.; Mori, H.; Pergushov, D. V.; Plamper, F. A. Temperature-Induced Structure Switch in Thermo-Responsive Micellar Interpolyelectrolyte Complexes: Toward Core−Shell−Corona and Worm-like Morphologies. *Soft Matter* **2016**, *12* (23), 5127−5137.
(94) Dähling, C.; Lotze, G.; Mori, H.; Pergushov, D. V.; Plamper, F. A. Thermoresponsive Segments Retard the Formation of Equilibrium Micellar Interpolyelectrolyte Complexes by Detouring to Various Intermediate Structures. *J. Phys. Chem. B* **2017**, *121* (27), 6739−6748.
(95) van Hees, I. A.; Swinkels, P. J. M.; Fokkink, R. G.; Velders, A. H.; Voets, I. K.; van der Gucht, J.; Kamperman, M. Self-Assembly of Oppositely Charged Polyelectrolyte Block Copolymers Containing Short Thermoresponsive Blocks. *Polym. Chem.* **2019**, *10* (23), 3127−3134.
(96) Voets, I. K.; Fokkink, R.; De Keizer, A.; May, R. P.; De Waard, P.; Cohen Stuart, M. A. On the Transition between a Heterogeneous and Homogeneous Corona in Mixed Polymeric Micelles. *Langmuir* **2008**, *24* (21), 12221−12227.
(97) Voets, I. K.; Fokkink, R.; Hellweg, T.; King, S. M.; Waard, P. De; De Keizer, A.; Cohen Stuart, M. A. Spontaneous Symmetry Breaking: Formation of Janus Micelles. *Soft Matter* **2009**, *5* (5), 999−1005.
(98) Synatschke, C. V.; Schacher, F. H.; Förtsch, M.; Drechsler, M.; Müller, A. H. E. Double-Layered Micellar Interpolyelectrolyte Complexes - How Many Shells to a Core? *Soft Matter* **2011**, *7* (5), 1714−1725.
(99) Betthausen, E.; Drechsler, M.; Förtsch, M.; Pergushov, D. V.; Schacher, F. H.; Müller, A. H. E. Stimuli-Responsive Micellar Interpolyelectrolyte Complexes − Control of Micelle Dynamics via Core Crosslinking. *Soft Matter* **2012**, *8* (39), 10167.
(100) Raya, R. K.; Štěpánek, M.; Limpouchová, Z.; Procházka, K.; Svoboda, M.; Lísal, M.; Pavlova, E.; Skandalis, A.; Pispas, S. Onion Micelles with an Interpolyelectrolyte Complex Middle Layer: Experimental Motivation and Computer Study. *Macromolecules* **2020**, *53* (16), 6780−6795.
(101) Fehér, B.; Zhu, K.; Nyström, B.; Varga, I.; Pedersen, J. S. Effect of Temperature and Ionic Strength on Micellar Aggregates of Oppositely Charged Thermoresponsive Block Copolymer Polyelectrolytes. *Langmuir* **2019**, *35* (42), 13614−13623.
(102) Dähling, C.; Houston, J. E.; Radulescu, A.; Drechsler, M.; Brugnoni, M.; Mori, H.; Pergushov, D. V.; Plamper, F. A. Self-Templated Generation of Triggerable and Restorable Nonequilibrium Micelles. *ACS Macro Lett.* **2018**, *7* (3), 341−346.

https://dx.doi.org/10.1021/acsmacrolett.0c00787
ACS Macro Lett. 2021, 10, 167−179

(103) Yeow, J.; Boyer, C. Photoinitiated Polymerization-Induced Self-Assembly (Photo-PISA): New Insights and Opportunities. *Adv. Sci.* **2017**, *4* (7), 1700137.
(104) Charleux, B.; Delaittre, G.; Rieger, J.; D'Agosto, F. Polymerization-Induced Self-Assembly: From Soluble Macromolecules to Block Copolymer Nano-Objects in One Step. *Macromolecules* **2012**, *45*, 6753−6765.
(105) Canning, S. L.; Smith, G. N.; Armes, S. P. A Critical Appraisal of RAFT-Mediated Polymerization-Induced Self-Assembly. *Macromolecules* **2016**, *49*, 1985−2001.
(106) Warren, N. J.; Armes, S. P. Polymerization-Induced Self-Assembly of Block Copolymer Nano-Objects via RAFT Aqueous Dispersion Polymerization. *J. Am. Chem. Soc.* **2014**, *136*, 10174−10185.
(107) Yu, Q.; Ding, Y.; Cao, H.; Lu, X.; Cai, Y. Use of Polyion Complexation for Polymerization-Induced Self-Assembly in Water under Visible Light Irradiation at 25 °C. *ACS Macro Lett.* **2015**, *4* (11), 1293−1296.
(108) Liu, Q.; Wang, X.; Ma, L.; Yu, K.; Xiong, W.; Lu, X.; Cai, Y. Polymerization-Induced Hierarchical Electrostatic Self-Assembly: Scalable Synthesis of Multicompartment Polyion Complex Micelles and Their Monolayer Colloidal Nanosheets and Nanocages. *ACS Macro Lett.* **2020**, *9* (4), 454−458.
(109) Shen, L.; Li, Y.; Lu, Q.; Qi, X.; Wu, X.; Zhou, Z.; Shen, J. Directed Arrangement of SiRNA: Via Polymerization-Induced Electrostatic Self-Assembly. *Chem. Commun.* **2020**, *56* (16), 2411−2414.
(110) Cai, M.; Ding, Y.; Wang, L.; Huang, L.; Lu, X.; Cai, Y. Synthesis of One-Component Nanostructured Polyion Complexes via Polymerization-Induced Electrostatic Self-Assembly. *ACS Macro Lett.* **2018**, *7* (2), 208−212.
(111) Aloi, A.; Guibert, C.; Olijve, L. L. C.; Voets, I. K. Morphological Evolution of Complex Coacervate Core Micelles Revealed by IPAINT Microscopy. *Polymer* **2016**, *107*, 450−455.
(112) Feiner-Gracia, N.; Olea, R. A.; Fitzner, R.; El Boujnouni, N.; van Asbeck, A. H.; Brock, R.; Albertazzi, L. Super-Resolution Imaging of Structure, Molecular Composition, and Stability of Single Oligonucleotide Polyplexes. *Nano Lett.* **2019**, *19* (5), 2784−2792.
(113) Riera, R.; Feiner-Gracia, N.; Fornaguera, C.; Cascante, A.; Borrós, S.; Albertazzi, L. Tracking the DNA Complexation State of PBAE Polyplexes in Cells with Super Resolution Microscopy. *Nanoscale* **2019**, *11* (38), 17869−17877.
(114) Ting, J. M.; Marras, A. E.; Mitchell, J. D.; Campagna, T. R.; Tirrell, M. V. Comparing Zwitterionic and PEG Exteriors of Polyelectrolyte Complex Micelles. *Molecules* **2020**, *25* (11), 2553.

https://dx.doi.org/10.1021/acsmacrolett.0c00787
ACS Macro Lett. 2021, 10, 167−179